THE JOURNAL OF PHYSICAL CHEMISTRY C

Article

pubs.acs.org/JPCC

Conformation and Dynamics of Organic Tethers Bound to MCM41-Type Surfaces from Solid State NMR Measurements

Lee Ghindes-Azaria,[†] Esthy Levy,[†] Keren Keinan-Adamsky, and Gil Goobes*

Department of Chemistry, Bar Ilan University, Ramat Gan 52900, Israel

Supporting Information

ABSTRACT: The conformation and motions of organic chains bound to the surface of MCM41-type mesoporous silica materials are investigated in molecular detail. 2D heteronuclear correlation measurements in conjunction with relaxation measurements are used to infer both the orientation and the motions of the organic chains on the silica surface. In octyl-MCM41, proximity of octyl tether carbons to silanols is observed with the exception of the terminal carbons, pointing to slight chain bending which positions the center carbons in the chain closer to neighboring silanols. In aminopropyl-MCM41, the carbon directly bound to the amine group is the closest to silanol protons and physisorbed water protons, indicating a tilted orientation of the tail allowing for the amine group to interact with the silanol. Motions in the two chains are characterized by using ^{13}C longitudinal and rotating frame relaxation measurements. Substantial differences in the T_1 and $T_{1\rho}$ times of the two materials are shown to be the result of differences in activation energy for respective rotation and libration motions between the two materials. The shorter tether in aminopropyl-MCM41, characterized by larger kinetic barriers for libration motions, demonstrates higher chain rigidity. The longer chain in octyl-MCM41 is characterized by faster librations and slower bond rotations in the center carbons. Evidence from structural and dynamical data jointly provides a detailed view of the chain behavior and underscores differences in the physical properties of the two tethers bound to the MCM41-type surface.

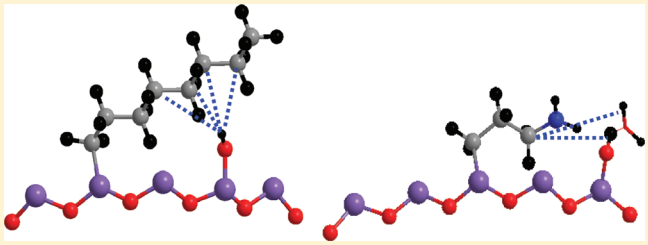

1. INTRODUCTION

Porous silica structures are common support materials in Nature[1] and in man-made applications.[2] Synthesis of mesoporous silica materials comprising a well ordered mesh of nanopores with tunable pore size[3−6] has paved the way for their employment in numerous applications. In addition, functionalization of their surface by simple attachment of organic groups has substantially expanded the chemical and physical properties of these materials, rendering them adjustable hydrophilic character, altered acidity and permeability, as well as other properties such as electrical conductivity. One of the common mesoporous silica materials, MCM41,[3,4] has been the target for extensive surface modification.[7,8] Modified MCM41 surfaces were utilized in preparation of highly reactive catalysis spots,[9,10] controlled synthesis of linear polymer nanofibers,[11] chromatography and immobilization of biomolecules for biosensing,[12,13] drug delivery and other applications.[14] These novel materials are not only interesting from a chemical viewpoint but also from a physical perspective, since they serve as molecular brushes confined to cavities of dimensions not much larger than the size of the tethered functional groups themselves having unique visco-elastic features that depend on the amount of solvent molecules in their close environment.

MCM41 is synthesized by silica polymerization on the surface of a template made of micellar nanorods followed by calcination to remove the template and by that to form the typical mesoporous architecture. Surface modifications of MCM41 are typically generated either via postpolymerization reaction of silanol groups on the surface of MCM41 with chlorosilane or alkoxysilane containing molecules[4,8,15] or by co-condensation of a standard precursor of silica with a precursor that has three alkoxy groups and one heterogroup. During condensation, the heterogroup does not participate in polymerization, remains unreacted, and resides on the pore walls and outer surfaces of the mesoporous structure as it forms.

It was previously shown that copolymerizing a blend of 80% tetraethoxysilane (TEOS) with 20% aminopropyl triethylsilane (ATES)[7,16,17] or 20% vinyl triethylsilane[18] results in mesoporous silica with MCM-41 architecture having aminopropyl or vinyl tethers respectively bound to the silica surfaces. For these surface modified mesoporous silica materials, it is highly desirable to determine the chemical and physical state of the surface groups. Surface chemical and physical characteristics are expected to vary markedly between different preparation approaches and depend on the end group properties. Modification using organic reagents was found to result in lower porosity and a change in the chemical properties of the surface such as hydrophobicity and acidity.[15] An MCM41 functionalized with a mixture of two organic tethers has shown a substantial resistance to hydrolysis in boiling water owing to

Received: December 28, 2011
Revised: February 23, 2012
Published: February 24, 2012

protection of the siloxane bonds in the silica framework by the organic moieties.[12]

It is valuable to determine the conformation and the motions of alkyl chains on the pore walls and outer surfaces and concurrently to elicit to what extent are the properties of host molecules within these materials altered. Previous work utilized solid state NMR techniques to investigate structural aspects of alkyl chain in allyl-MCM41-type material.[19] The allyl groups were shown to be covalently linked to the silica surface, to interact strongly with both bulk and surface silicon atoms, and to reside in the vicinity of adsorbed water molecules. Some dynamic information regarding the allyl chain was inferred from cross-polarization dynamics measurements; however, no quantitative assessment was carried out. Recently, it was also shown that indirect detection can be helpful in shortening signal acquisition times in 2D $^{13}C-^{1}H$ correlation experiments without loss of resolution in similar functionalized MCM41-type materials.[20]

In this study, we investigate and compare both structural and dynamic aspects of the organic tethers quantitatively in two functionalized MCM41-type materials prepared by co-condensation of the standard TEOS and organosiloxane precursors. The first material is ap-MCM41 prepared from the precursor aminopropyl triethoxysilane (ATES) which links hydrophilic tethers to the silica surfaces. This silica material is easily suspended in water and is also prone to spontaneous water permeation in air. The other material is o-MCM41 based on the precursor octyl triethoxysilane (OTES) which produces octyl tethers on the mesoporous silica. This material shows hydrophobic character, does not suspend in water, and has a very low level of water permeation under atmosphere of air. We report ^{1}H spectra of the two materials recorded under $^{1}H-^{1}H$ decoupling using window-phase-modulated Lee−Goldburg (wPMLG) to resolve the tether and silanol proton lines and to point out the sources of line broadening for the adsorbed water molecules in these materials. Two-dimensional proton−carbon correlation spectra employing phase-modulated Lee−Goldberg (PMLG) decoupling during t_1 are used to detect the proximity of the side chain to silanol and physisorbed water protons and from that to infer details of the organic tethers conformation relative to groups on the silica surface.

Longitudinal and rotating frame ^{13}C relaxation of the octyl and aminopropyl chains extending from the silica framework are recorded as a function of temperature. These two relaxation measurements are sensitive to dynamics at different time scales and therefore give a complementary quantitative characterization of the motions in the two tethers. They are shown here to reflect the chain length and to some extent also the chemical environment influencing the interaction of the tethers with the silica surface environment. The combination of conformation and motional observations helps us to define the physical state of the chains on the surfaces of the silica.

2. EXPERIMENTAL SECTION

Sample Preparation. Syntheses of o-MCM41 and ap-MCM41[7] were carried out at room temperature from mixtures containing a constant molar ratio of the organotrialkoxysilane (either ATES or OTES) with tetraethoxysilane (TEOS) in the presence of the surfactant C_{16}TAB. A solution composed of a molar ratio Si/C_{16}TAB/H_2O/NH_4OH of 1.0:0.12:130.1:0.5 was prepared. Typically, a solution was made of water (2.34 g, 0.13 mol), ammonium hydroxide (0.02 g, 0.5 mmol), and C_{16}TAB (0.044 g, 0.12 mmol). The surfactant was dissolved by warming the solution to 40 °C. Then, a mixture containing the organotrialkoxysilane and TEOS in 2:8 molar ratio was added dropwise to this solution under rapid stirring. The organotrialkoxysilane and TEOS were mixed, and the mixture was added to the surfactant solution. Once the solution had homogenized, the stirring was slowed for an additional 10 min. After aging at 80 °C for 4 days, the product was extracted by filtration as a white powder.

Surfactant Extraction. Standard calcination at elevated temperatures was avoided in these organically modified minerals. The surfactant template was removed from the organosilica materials, instead, through a solvent extraction process. A 2 g sample of product was refluxed in 3 mL of HCl (37 wt %) and 200 mL of methanol for 2 days, collected by suction filtration, washed with water, and dried in air at room temperature.

NMR Measurements. All measurements were carried out on a Bruker Avance^{III} 500 MHz spectrometer using a double tuned 4 mm MAS probe. ^{1}H direct excitation experiments were carried out using 109 kHz 90° pulses, at a spinning rate of 10 kHz. Window-phase-modulated Lee−Goldberg experiments were carried out at an effective field of 105 kHz using PMLG5 employing a set of 10 discrete phases with super cycling and discrete acquisition windows.[21] These experiments were carefully calibrated on a standard glycine sample prior to each measurement on the porous silica materials. Typical scaling factors used in supercycled wPMLG experiments (0.47) were employed during data processing. T_1 inversion recovery experiments were carried out using inversion and detection pulses of 38 kHz and SPINAL[22] decoupling of 90 kHz, at a spinning rate of 10 kHz. $T_{1\rho}$ experiments were carried out using initial carbon excitation with ramped CP for 1400 μs from protons at a field of 37 kHz on ^{13}C and between 38.3 and 76.5 kHz on ^{1}H at a spinning rate of 10 kHz, followed by variable duration carbon spin lock at a field of 38.3 kHz for o-MCM41 and 14.4 kHz for ap-MCM41 and using SPINAL decoupling at 90 kHz during spin lock and acquisition periods. 2D $^{1}H-^{13}C$ heteronuclear correlation experiments were carried out using PMLG5 decoupling at an effective field of 105 kHz during ^{1}H evolution in T_1 followed by polarization transfer from ^{1}H to ^{13}C with mixing times of 500 and 1500 μs, at a spinning rate of 11 kHz and using SPINAL decoupling at a field of 90 kHz during signal acquisition. 2D experiments using 256 t_1 points were taken, and each point was signal averaged 1024 times. NMR pulse schemes used are shown in Figure 1s in the Supporting Information. Inversion recovery experiments were carried out using recycle delays of 30 s and its fast acquisition analogue[23] using 5s. All other experiments started with ^{1}H excitation and were carried out with a recycle delay of 1 s.

3. RESULTS AND DISCUSSION

Characterization of o-MCM41 and ap-MCM41. Small angle X-ray diffraction measurements were recorded using a Bruker AXS diffractometer equipped with a Cu Kα source emitting at λ = 1.5418 Å. High resolution transmission electron micrographs were collected on a Jeol 2100 microscope equipped with a US4K CCD camera using a tungsten filament as the electron source accelerated at 200 kV. Typical small-angle X-ray diffraction patterns characteristic of MCM-type structure and high resolution transmission electron micrographs showing the pore dimensions for the two materials are provided in Figure 2s and Tables 1s and 2s in the Supporting

dx.doi.org/10.1021/jp212524f | J. Phys. Chem. C 2012, 116, 7442−7449

Information. In o-MCM41 besides the mesoporous structures, there is some evidence for small pores in the order of 2 nm.

The amount of alkyl tethers on the silica surface in the final products was inferred from ^{29}Si CPMAS measurements (data not shown). The relative intensity of the T-band representing surface Si atoms having Si−C bonds versus the Q-band representing typical silica surface groups of the form $Si(OH)_n(OSi)_{4-n}$[7] gave rise to 29 and 24% of surface Si atoms having an alkyl tether attached in ap-MCM41 and o-MCM41, respectively. These values are a little high based on the 20 mol % alkyl precursor used in the synthesis; however, they report on an efficient incorporation of the precursor onto the silica surface upon condensation.

The ^{1}H spectrum of both o-MCM41 and ap-MCM41 after template removal by acid-reflux should be comprised of resonances that are typically seen in unmodified MCM41 as well as resonances from the octyl and aminopropyl groups bound to inner and outer surfaces of the silica. Silanol groups prevalent on the silica surfaces give rise to lines at shifts as low as 1.75 ppm for isolated silanols and as high as 3.4 ppm for silanols undergoing ^{1}H exchange with surrounding water molecules.[24] Water molecules either occupying vacancies inside the silica framework or adsorbed onto its outer surfaces give rise to shifts between 4.5 and 5.6 ppm depending on the specific surface properties at different locations.[25] Acidic proton resonances observed at 6.0−8.5 ppm are also typically observed as reported before.[26] These species are probably formed as a result of the attachment of H^+ to silanol oxygen lone pairs and the formation of $Si-OH_2^+$ species on the silica surfaces. Shielded protons in the organic tethers are expected at low chemical shifts.

^{1}H NMR Data of o-MCM41. The 90°-acquire ^{1}H spectrum (blue) of o-MCM41 is shown in Figure 1a. Line assignments detailed below are aided by spectral deconvolution using DMFIT[27] are given in Figure 3s and Table 3s in the Supporting Information. The 12 methylene protons in the center of the octyl tether, on carbons C2−C7 (see inset in Figure 2), give rise to two lines at 1.00 and 1.35 ppm having similar intensities. These protons are slightly shifted (∼0.1−0.2 ppm) relative to analogous protons in the OTES monomer which appear at 1.19 and 1.24 ppm in solution. The three protons of the methyl group and last pair of methylene protons on C1 attached directly to the silica ($Si-CH_2$) give rise to a broad line at 0.4 ppm. The intensity ratio between the latter line and the two former lines is 0.3, which slightly deviates from the expected ratio of 0.4. Nonexchanging silanol protons are observed at 1.8 and water exchangeable silanol protons at 3.2 ppm. The latter silanol line makes only 1% of the total spectral intensity. The water line could not be fitted satisfactorily to a single line. Instead, it is better represented by two overlapping water lines having similar amplitude at 4.5 and 4.7 ppm. Further confirmation of this assignment is made by measurement at slightly different hydration levels of the material (data not shown) which gives rise to disparate population of the two water sites. Similarly, the acidic proton band is composed of two lines at 6.1 and 7.5 ppm.

The window-phase-modulated Lee−Goldburg (wPMLG) experiments are used here in order to obtain homonuclear decoupled ^{1}H spectra of the materials. The wPMLG spectrum of o-MCM41 is shown in Figure 1a (red) as well. Comparing the two spectra, we observe narrowing of the octyl proton lines exposing the nonexchangeable silanol line at 1.8 ppm. The water resonance, on the other hand, retains its full width at half-maximum but appears reduced in intensity relative to the octyl protons. The fact that the water line width is left unchanged under ^{1}H−^{1}H decoupling indicates that water protons in this sample do not experience strong persistent couplings to neighboring water protons or any other protons. The source of the relatively broad water line may either be from fast transverse relaxation or due to chemical shift dispersion. The latter possibility may suggest that several chemically inequivalent adsorption sites are occupied by water molecules on o-MCM41 surfaces.

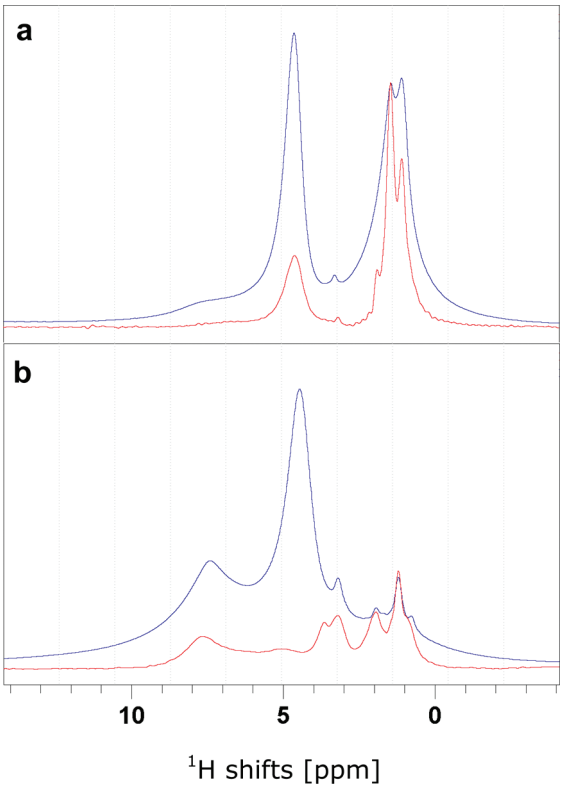

Figure 1. ^{1}H 90°-acquire (blue) and wPMLG (red) spectra of o-MCM41 (a) and ap-MCM41 (b).

^{1}H NMR Data of ap-MCM41. The 90°-acquire ^{1}H spectrum (blue) of ap-MCM41 is shown in Figure 1b. The methylene protons on carbons C1, C2, and C3 in the aminopropyl tether give rise to three lines with similar intensity at 0.8, 1.2, and 3.2 ppm, respectively. These protons are shifted by 0.25, −0.2, and 0.7 ppm with respect to analogous protons in the ATES monomer. Spectral deconvolution along with line width and chemical shift data are given in Figure 4s and Table 4s in the Supporting Information. A broad line due to nonexchangeable silanols, though not resolved, appears at 1.7 ppm. Here again, the water resonance is better fitted to two lines at 4.5 and 4.8 ppm and the acidic protons to two resonances at 6.0 and 7.6 ppm that are more intense than in the o-MCM41 material.

The wPMLG spectrum (red) of ap-MCM41 is shown in Figure 1b as well. The tether protons exhibit broader lines than in the 90°-acquire spectrum, but the 2.0 ppm silanol line is better resolved. The 3−4 ppm region has another line revealed at 3.7 ppm due to severe attenuation of the water resonances. This line is attributed to highly mobile physisorbed water.[26] The attenuation of the water resonance at 4.5 ppm exposes the water line at 4.8 ppm which represents static water molecules. The acidic proton line at 7.6 ppm is much less attenuated by

dx.doi.org/10.1021/jp212524f | J. Phys. Chem. C 2012, 116, 7442−7449

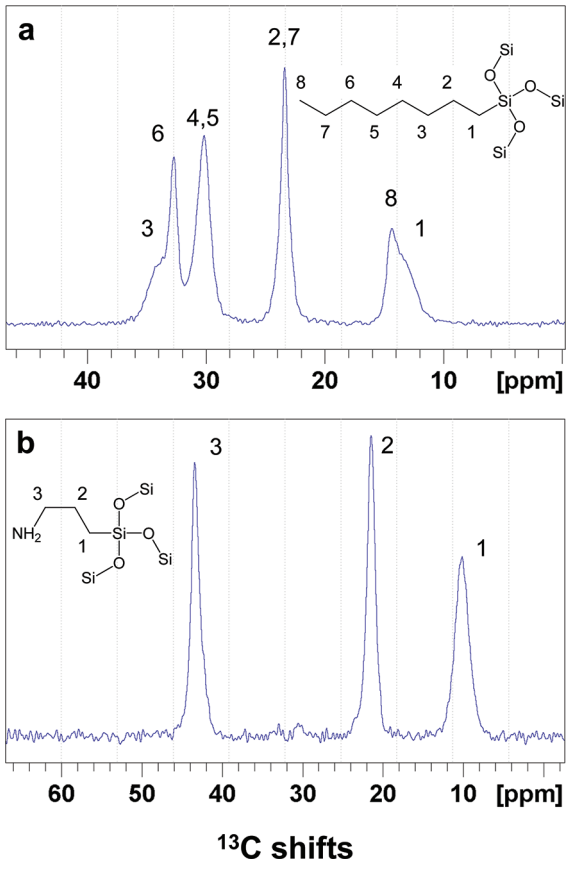

Figure 2. ^{13}C CPMAS spectra of o-MCM41 (a) and ap-MCM41 (b) shown with the chemical formula of respective tethers with carbons in the insets and in the spectra enumerated.

decoupling as compared to the same line in the wPMLG spectrum of o-MCM41.

Comparing ^{1}H NMR Spectra of the Two Materials. In the ap-MCM41 90°-acquire spectrum, the tether resonances have a much lower line intensity (3%) as compared to the tether resonances in o-MCM41 (37%). This is a consequence of more extensive adsorption of water onto the hydrophilic surfaces of ap-MCM41 over time. Another visible difference is a stronger acidic proton band in ap-MCM41 relative to o-MCM41. This is attributed to the presence of NH_3^+ protons on the ap-MCM41 tether readily available to form hydrogen bonds with adjacent silanols. Spectra of both materials exhibit the typical nonexchangeable silanol sites observed for native MCM41 at appreciable amounts and interestingly negligible or unobserved amounts of exchangeable silanols. This information and further experiments detailed hereafter are used to capture the tether orientation on the silica surface of both hydrophilic ap-MCM41 and hydrophobic o-MCM41.

The increased line width of the ap-MCM41 tether protons and substantial attenuation of the water line in the homonuclear decoupled spectra of the two materials is attributed to motions which occur in the time-scale of the wPMLG characteristic times. Under such circumstances, the coherent averaging by the decoupling pulses may be disrupted by the motions, leading to inefficient decoupling and broadening of the lines. Similar work describing the effects of molecular motions in the course of CRAMPS experiments was reported before.[28] Here, we observe that some lines are getting narrower in the wPMLG experiment while others are getting broader, indicating motions of the two tethers occur in different times scales, and in particular, the water dynamics is different than that for either silanol or tether protons.

^{13}C NMR Data of o-MCM41 and ap-MCM41. The ^{13}C cross-polarization magic angle spinning (CPMAS) spectrum of o-MCM41 is shown in Figure 2a. Assignment of the peaks to the eight carbons in the octyl tether (see inset) is straightforward. Small chemical shift differences (<0.4 ppm) between the end material and the OTES precursor (data not shown) are observed, except for the carbon directly bonded to the silica framework (denoted as C1) which exhibits a downfield shift of 2.7 ppm. Previous work on octyl tethers chemically linked to the surface of silica gel particles showed very similar carbon chemical shifts but uniform line width.[29] In the o-MCM41 spectrum, C1 and C3 with respective linewidths of 1.7 and 2.0 ppm exhibit nearly twice broader lines compared to other carbons in the tether and to the same carbons in the silica gel tether.[29]

The ^{13}C spectrum of ap-MCM41 is shown in Figure 2b with the three aminopropyl carbons appearing at 10.2, 21.6, and 43.4 ppm. The most shielded line is due to the carbon directly bonded to the silica framework (denoted as C1), whereas the least shielded, C3, belongs to the carbon bonded to the amine group. In analogy to the o-MCM41 case, the C1 (line width 1.9 ppm) is about twice as broad as the C2 and C3 lines (line width 1.1 ppm). Spectra of an aminopropyl tether attached to a silica gel surface exhibiting similar chemical shifts and broader lines have been reported before.[26,30] For both o-MCM41 and ap-MCM41 materials, the C1 line, serving as the anchor point of the tether to the surface of the silica, is consistently broader than other carbon lines. The larger chemical shift dispersion may be a consequence of the tether being attached to different points on the MCM41 surface which constitute disparate local environments. Direct excitation ^{13}C spectra of these materials (data not shown) contain similar intensities and shifts to the ones in the CP spectra shown in Figure 2.

2D $^{1}H-^{13}C$ Correlation Measurements of o-MCM41 and ap-MCM41. Two-dimensional spectra correlating the protons in the two materials with the tether carbons were measured using ^{1}H evolution in t_1 under PMLG decoupling conditions followed by polarization transfer using CP at different mixing times. Figure 3a shows 2D $^{1}H-^{13}C$ heteronuclear correlation (HETCOR) data of o-MCM41 at 500 (red) and 1500 μs (blue). Polarization transfer from methylene protons at both 1.0 and 1.35 ppm to tether carbons is observed with the latter showing more pronounced transfer. Transfer to C1 and C8 from these protons is the smallest, giving rise to weaker cross-peaks as expected. At the longer mixing time, polarization transfer to all carbons is nearly uniform and, in addition, magnetization transfer between the nonexchangeable silanol protons and tether carbons is also observed as the three cross-peaks along 1.8 ppm in F1. However, there is no magnetization transfer observed between the exchangeable silanol protons at 3.2 ppm and the tether carbons, which could be merely due to low population of the exchangeable silanol protons (only 1%) as observed in the ^{1}H spectrum of the material. C1−C3 and C8 on the head and tail of the tether do not show cross-peaks with silanol protons. Figure 3b shows $^{1}H-^{13}C$ correlation data for ap-MCM41 at mixing times of 500 (blue) and 1500 μs (red). Magnetization transfer between the three carbons and their respective directly bonded protons at 0.8, 1.2, and 3.2 ppm are observed at a mixing time of 500 μs. A large cross-peak between the

dx.doi.org/10.1021/jp212524f | J. Phys. Chem. C 2012, 116, 7442−7449

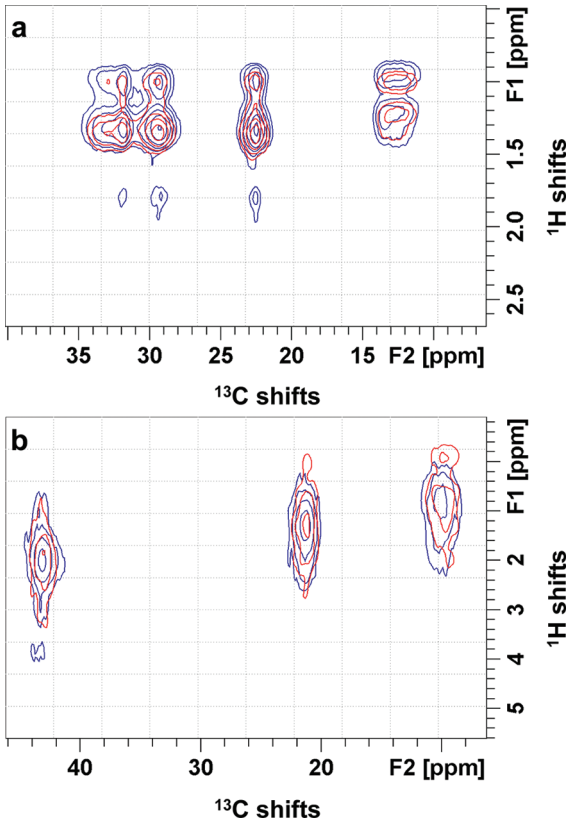

Figure 3. $^{1}H-^{13}C$ 2D HETCOR spectra of o-MCM41 (a) and ap-MCM41 (b) using 500 μs (red) and 1500 μs (blue) CP times. 2D spectra were acquired using 206 T_1 points over 36 h.

nonexchangeable silanol (2.0 ppm) and C3 is clearly visible, and smaller cross-peaks with C1 and C2 can also be seen and may explain the relatively broad lines in the F1 dimension. At a longer mixing time, a new cross-peak with the 3.7 ppm physisorbed water protons appears.

In o-MCM41, proximity of octyl tether carbons to silanols with the exception of the terminal carbons points to slight chain bending which positions carbons 4–7 closer to neighboring silanols. In ap-MCM41, the terminal carbon bound directly to the amine group is proximate to the silanol and to physisorbed water protons. The proximity to the silanol indicates that the chain is tilted and nearly laying flat on the surface to allow for the tail amine group to interact with the silanol.

Moreover, detectable correlations between the tether carbons and silanol protons reduce the chances that the organic tethers cluster on the surface of the silica. Such clusters may be thought to form during the copolymerization stage of the synthesis of porous organosilicas in particular for o-MCM41; however, the NMR results indicate that a significant portion of tethers is involved in interaction with surface silanols. In the o-MCM41 material, proximity of water molecules to tail carbons was not detected. This may be as a result of absence of vicinal water molecules from the direct environment of its hydrophobic tethers or due to fast exchange processes experienced by water molecules which hinders efficient transfer of polarization to tether carbons. In the latter case, lowering the temperature or evacuating a large portion of the water molecules may help detect proximity of water protons to tether carbons.

^{13}C Relaxation Data and Dynamics of o-MCM41 and ap-MCM41. Measurement of longitudinal and rotating-frame relaxation times can report on the molecular motions of the organic tethers at different time scales. Typically, longitudinal relaxation time (T_1) is sensitive to stochastic rotational motions around bonds with correlation times in the nanosecond regime and rotating-frame relaxation time ($T_{1\rho}$) can be used to track slower stochastic libration motion in the microsecond to millisecond time scale. Carbon T_1 and $T_{1\rho}$ measurements were carried out on o-MCM41 and ap-MCM41 at temperatures between 230 and 310 K. Relaxation data were analyzed on the basis of Bloembergen's relaxation treatment[31] assuming Arrhenius dependence of correlation times on temperature.[32] The dominant spin interactions governing return to equilibrium are assumed to be the $^{1}H-^{13}C$ dipolar interactions. Three parameters are invoked in each relaxation model. The activation energy and pre-exponential factor in Arrhenius' equation reflect the temperature dependence of the correlation times. The K and K' prefactors in eqs 1 and 2, respectively, account for the net effect of all the dipolar interactions that induce the energy transfer during the two relaxation processes.[33] Typical plots of $\ln(\tau)$ versus the inverse of the temperature (see example in Figure 5s in the Supporting Information) are constructed to extract the activation energy, E_a, and the pre-exponential factor, A. Parameters derived from the relaxation models are summarized in Tables 1 and 2.

$$\frac{1}{T_1^C} = K\{J_0(w_H - w_C) + 3J_1(w_C) + 6J_2(w_H + w_C)\}$$

$$J(w) = \frac{2\tau}{1 + w^2\tau^2} \quad (1)$$

The expression for the longitudinal rotating frame relaxation (eq 2) is simplified by neglecting the static field dependent term.

$$\frac{1}{T_{1\rho}^C} \cong K'\frac{\tau'}{1 + w_1{}^2\tau'^2} \quad (2)$$

In Figure 4, the temperature dependences of T_1 (left) and $T_{1\rho}$ (right) for the various carbons in the octyl tail are shown along with the corresponding simulated curves. Measured T_1 times follow a trend of consistently getting shorter for the carbons

Table 1. T_1 and $T_{1\rho}$ Relaxation Parameters of the Different Carbon Species in o-MCM41

	T_1			$T_{1\rho}$		
chemical identity	K	E_a (kJ/mol)	A (Hz)	K'	E_a (kJ/mol)	A (Hz)
C1	5.0×10^7	5.8	9.8×10^8	2.6×10^6	6.6	2.4×10^6
C2 + C7	6.4×10^7	10.7	5.9×10^{10}	2.6×10^6	2.5	3.2×10^5
C3	1.8×10^8	10.0	1.0×10^{11}	4.1×10^6	3.8	6.2×10^5
C4+ C5	9.9×10^7	13.3	2.4×10^{11}	1.6×10^7	2.5	1.5×10^6
C6	7.2×10^7	12.7	1.6×10^{11}	1.8×10^7	5.4	1.3×10^7
C8	5.2×10^7	7.2	2.5×10^{10}	2.6×10^7	8.1	4.9×10^7

dx.doi.org/10.1021/jp212524f | J. Phys. Chem. C 2012, 116, 7442–7449

Table 2. T_1 and $T_{1\rho}$ Relaxation Parameters of the Different Carbon Species in ap-MCM41

	T_1			$T_{1\rho}$		
chemical identity	K	E_a (kJ/mol)	A (Hz)	K'	E_a (kJ/mol)	A (Hz)
C1	9.30×10^7	4.1	4.00×10^8	8.34×10^6	16.8	1.20×10^8
C2	6.90×10^7	4.9	8.30×10^8	9.92×10^6	16.2	1.30×10^8
C3	6.00×10^7	6.1	1.20×10^9	9.39×10^6	15	6.50×10^7

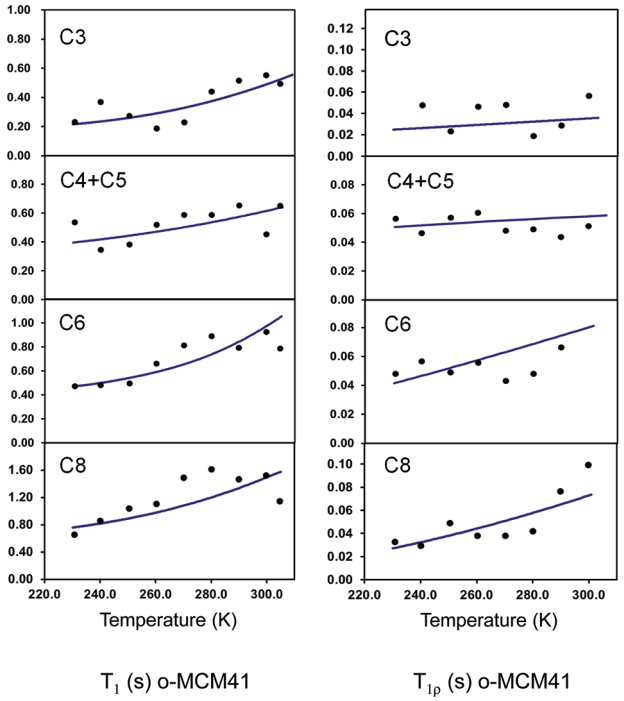

Figure 4. Experimental T_1 (left) and $T_{1\rho}$ (right) times in seconds versus temperature (symbols) together with calculated curves (lines) for the various carbons in the octyl tether in o-MCM41.

closer to the anchoring silicon atom along the chain. Similar behavior was observed for octyl carbons tethered to silica gel surfaces. The effect was attributed to methyl group rotations influencing the relaxation of adjacent carbons.[29] $T_{1\rho}$ times, on the other hand, follow an opposite trend of getting shorter for carbons farther away from the silica framework, with the exception of C3. The parameters used to fit the relaxation data of carbons C1, C2, and C7 are also given in Table 1 but are not displayed in the figure for the sake of clarity.

The temperature dependences of carbon T_1 (left) and $T_{1\rho}$ (right) in the aminopropyl tether are shown in Figure 5 with the simulated curves. Conversely to the octyl tether, ^{13}C T_1 times in ap-MCM41 decrease with temperature but again become slightly longer the farther the carbon is from the silica surface, in accordance with an increase in motional degrees of motion. The $T_{1\rho}$ times increase with temperature and show almost no variation between the different carbons. Another prominent difference between the two materials is the average $T_{1\rho}$ value which in o-MCM41 is ca. 0.05 s and in ap-MCM41 is nearly an order of magnitude lower owing to the higher chain rigidity in the latter. Average T_1 correlation times are in the range of 1−3 ns for o-MCM41 except for C1 (14 ns) and nearly an order of magnitude larger for ap-MCM41 (13−18 ns). $T_{1\rho}$ correlation times are split between 0.9 μs for C6, C8, C4, and C5 and 8.5−10 μs for C1, C2 and C7, C3 in o-MCM41. $T_{1\rho}$ correlation times in ap-MCM41 are 18−25 μs for the three carbons. These times are dependent on values of w_1

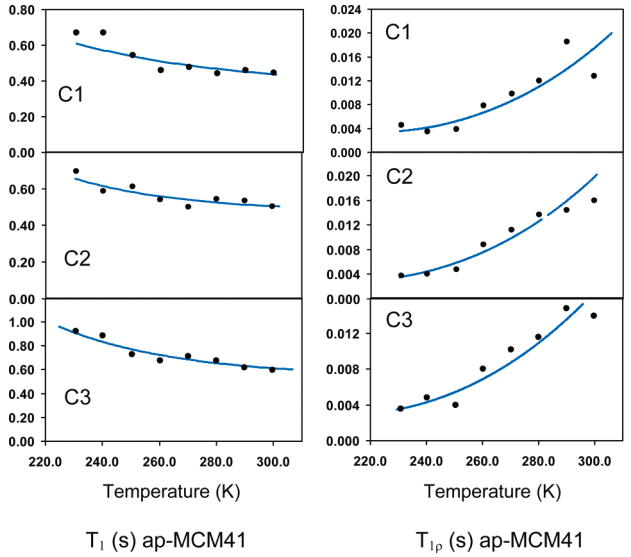

Figure 5. Experimental T_1 (left) and $T_{1\rho}$ (right) times in seconds versus temperature (symbols) together with calculated curves (lines) for the various carbons in the aminopropyl tether in ap-MCM41.

fields used in the experiments and reported in the Experimental Section. Errors in the activation energies derived from the T_1 and $T_{1\rho}$ data are 15 and 20% for o-MCM41 T_1 and $T_{1\rho}$ data, respectively, and 8 and 11% for ap-MCM41 T_1 and $T_{1\rho}$ data, respectively. The model used to extract the dynamics assumes that phase transitions such as freezing of the surrounding water molecules do not take place at temperatures used in the measurement. It would be intriguing to investigate the chain dynamics at lower temperatures and at different levels of pore filling by the solvent molecules as different layers of solvent molecules occupying the pores might be characterized themselves by different motions.

4. CONCLUSIONS

Molecular structure and dynamics of octyl and aminopropyl tethers bound to the surface of MCM41-type mesoporous silica materials were characterized using ^1H and ^{13}C MAS NMR measurements. Proximity measurements indicated the orientation of organic chains with respect to surface groups as shown in the simplified model in Figure 6. The octyl tail is proximate to isolated silanols which are more prevalent on the hydrophobic surfaces of o-MCM41 silica, while the aminopropyl tail is close enough to interact with both silanols and physisorbed water. Adsorbed water molecules may be mediating hydrogen bonds between the amine and silanol groups.

Motions of the organic tail were extracted from relaxation measurements and provided with defining properties of the two chains. The pronounced differences in ^{13}C longitudinal and rotating frame relaxation times between the two materials were linked to differences in activation energy for rotation and

dx.doi.org/10.1021/jp212524f | J. Phys. Chem. C 2012, 116, 7442−7449

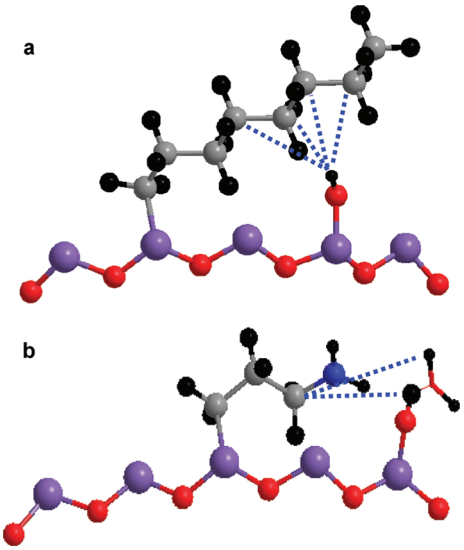

Figure 6. Models showing bending of the organic tethers relative to silanol groups on the silica surface in o-MCM41 (a) and in ap-MCM41 (b). Different atoms are colored as follows: Si (purple), O (red), N (blue), C (gray), and H (black).

libration motions, respectively, in the aminopropyl tails compared to the octyl tails. The shorter aminopropyl tether shows higher chain rigidity due to a larger kinetic barrier for libration. The lower activation energy in octyl-MCM41 is translated into faster librations in the center carbons. Concurrently, higher rotational activation energy in the center carbons gives rise to slower rotations around the C−C bonds.

■ ASSOCIATED CONTENT

Ⓢ Supporting Information

Characterization of the mesoporous materials, data analysis, pulse schemes, figures, and tables. This material is available free of charge via the Internet at http://pubs.acs.org.

■ AUTHOR INFORMATION

Corresponding Author

*E-mail: gil.goobes@biu.ac.il.

Author Contributions

†These authors contributed equally.

Funding

This research study was supported by the Crown Family foundation career development fellowship for young investigator.

Notes

The authors declare no competing financial interest.

■ ACKNOWLEDGMENTS

The authors thank Professor Yitzhak Mastai for kindly providing us with the ap-MCM41 and o-MCM41 materials used in this work. The authors also thank Dr Michal Leskes and Professor Shimon Vega for useful discussions.

■ ABBREVIATIONS

OTES, octyltriethoxysilane; ATES, aminopropyltriethoxysilane; TEOS, tetraethoxysilane; o-MCM41, octyl tethered MCM41-type silica; ap-MCM41, aminopropyl tethered MCM41-type silica; CP, cross-polarization; PMLG, phase-modulated Lee−Goldburg; HETCOR, heteronuclear correlation

■ REFERENCES

(1) Round, F. E.; Crawford, R. M. *The Diatoms. Biology and Morphology of the Genera*; Cambridge University Press: Cambridge, U.K., 1990.

(2) (a) Xu, R.; Pang, W.; Yu, J. *Chemistry of zeolites and related porous materials: synthesis and structure*; Wiley-Interscience: 2007. (b) Corma, A. *Chem. Rev.* **1997**, *97*, 2373−2419. (c) Giraldo, L. F.; Lopez, B. L.; Perez, L.; Urrego, S.; Sierra, L.; Mesa, M. *Macromol. Symp.* **2007**, *258*, 129.

(3) Beck, J. S.; Vartuli, J. C.; Roth, W. J.; Leonowicz, M. E.; Kresge, C. T.; Schmitt, K. D.; Chu, C. T. W.; Olson, D. H.; Sheppard, E. W.; McCullen, S. B.; Higgins, J. B.; Schlenker, J. L. *J. Am. Chem. Soc.* **1992**, *114*, 10834.

(4) Zhao, X. S.; Lu, G. Q.; Millar, G. J. *Ind. Eng. Chem. Res.* **1996**, *35*, 2075.

(5) Zhao, D.; Feng, J.; Huo, Q.; Melosh, N.; Fredrickson, G. H.; Chmelka, B. F.; Stucky, G. D. *Science* **1998**, *279*, 548.

(6) Che, S.; Garcia-Bennett, A. E.; Yokoi, T.; Sakamoto, K.; Kunieda, H.; Terasaki, O.; Tatsumi, T. *Nat. Mater.* **2003**, *2*, 801.

(7) Fowler, C. E.; Burkett, S. L.; Mann, S. *Chem. Commun.* **1997**, *18*, 1769.

(8) Yasmin, T.; Muller, K. *J. Chromatogr., A* **2010**, *1217*, 3362.

(9) (a) Jones, M. D.; Duer, M. J.; Hermans, S.; Khimyak, Y. Z.; Johnson, B. F. G.; Thomas, J. M. *Angew. Chem., Int. Ed.* **2002**, *41*, 4726. (b) Hermans, S.; Raja, R.; Thomas, J. M.; Johnson, B. F. G.; Sankar, G.; Gleeson, D. *Angew. Chem., Int. Ed.* **2001**, *40*, 1211.

(10) (a) Zhou, W.; Thomas, J. M.; Shephard, D. S.; Johnson, B. F. G.; Ozkaya, D.; Maschmeyer, T.; Bell, R. G.; Ge, Q. *Science* **1998**, *280*, 705−708. (b) Martin-Aranda, R. M.; Cejka, J. *Top. Catal.* **2010**, *53*, 141.

(11) Kageyama, K. K.; Tamazawa, J.; Aida, T. *Science* **1999**, *285*, 2113.

(12) Luechinger, M.; Prins, R.; Pirngruber, G. D. *Microporous Mesoporous Mater.* **2005**, *85*, 111.

(13) (a) Diaz, J. F.; Balkus, K. J. Jr. *J. Mol. Catal. B: Enzym.* **1996**, *2*, 115. (b) Yang, J.; Stevens, G. W.; O'Connor, A. J. *J. Aust. Ceram. Soc.* **2008**, *44*, 1.

(14) (a) Manzano, M; Aina, V.; Areao, C. O.; Balas, F.; Cauda, V.; Colilla, M; Delgado, M. R.; Vallet-Regi, M. *Chem. Eng. J.* **2008**, *137*, 30. (b) Davis, M. E. *Nature* **2002**, *417*, 813. (c) Cai, Q.; Zou, W. Y.; Luo, Z. S.; Wen, Q. X.; Pang, W. Q.; Cui, F. Z. *Mater. Lett.* **2003**, *58*, 1.

(15) Zhao, X. S.; Lu, G. Q.; Hu, X. *Microporous Mesoporous Mater.* **2000**, *41*, 37.

(16) Levy, E.; Kolesnikov, A. I.; Li, J.; Mastai, Y. *Surf. Sci.* **2009**, *603*, 71.

(17) Levy, E.; Chan, L. K.; Yu, D.; Koza, M. M.; Mastai, Y.; Ford, R. C.; Li, J. *J. Solid State Chem.* **2010**, *183*, 1691.

(18) Lim, M. H.; Blanford, C. F.; Stein, A. *J. Am. Chem. Soc.* **1997**, *119*, 4090.

(19) Trebosc, J.; Wiench, J. W.; Huh, S.; Lin, V. S. -Y.; Pruski, M. *J. Am. Chem. Soc.* **2005**, *127*, 7587.

(20) (a) Mao, K.; Wiench, J. W.; Lin, V.S.-Y.; Pruski, M. *J. Magn. Reson.* **2009**, *196*, 92. (b) Wiench, J. W.; Bronnimann, C. E.; Lin, V.S.-Y.; Pruski, M. *J. Am. Chem. Soc.* **2007**, *129*, 12076.

(21) Leskes, M.; Madhu, P. K.; Vega, S. *J. Chem. Phys.* **2007**, *447*, 370.

(22) Brauniger, T.; Wormald, P.; Hodgkinson, P. *Monatsh. Chem.* **2002**, *133*, 1549.

(23) Gupta, R. K.; Ferretti, J. A.; Becker, E. D.; Weiss, G. H. *J. Magn. Reson.* **1980**, *38*, 447.

(24) Grunberg, B.; Emmler, T.; Gedat, E.; Shenderovich, I.; Findenegg, G. H.; Limbach, H. H.; Buntkowsky, G. *Chem.—Eur. J.* **2004**, *10*, 5689.

(25) Trebosc, J.; Wiench, J. W.; Huh, S.; Lin, V. S. -Y.; Pruski, M. *J. Am. Chem. Soc.* **2005**, *127*, 3057.

(26) (a) Amitay-Rosen, T.; Kababya, S.; Vega, S. *J. Phys. Chem. B* **2009**, *113*, 6267. (b) Caravajal, G. S.; Leyden, D. E.; Quinting, G. R.; Maciel, G. E. *Anal. Chem.* **1988**, *60*, 1776.

(27) Massiot, D.; Fayon, F.; Capron, M.; King, I.; Le Calvé, S.; Alonso, B.; Durand, J. O.; Bujoli, B.; Gan, Z.; Hoatson, G. *Magn. Reson. Chem.* **2002**, *40*, 70.
(28) Liu, C. C.; Maciel, G. E. *Anal. Chem.* **1996**, *68*, 1401.
(29) Sindorf, D. W.; Maciel, G. E. *J. Am. Chem. Soc.* **1983**, *105*, 1848.
(30) Huh, S.; Wiench, J. W.; Yoo, J.-C.; Pruski, M.; Lin, V. S.-Y. *Chem. Mater.* **2003**, *15*, 4247.
(31) Bloembergen, N.; Purcell, E. M.; Pound, R. V. *Phys. Rev.* **1948**, *73*, 679.
(32) Torchia, D. A.; Szabo, A. *J. Magn. Reson.* **1982**, *49*, 107.
(33) Pizzanelli, S.; Kababya, S.; Frydman, V.; Landau, M.; Vega, S. *J. Phys. Chem. B* **2005**, *109*, 8029.